Available online at www.sciencedirect.com
SCIENCE DIRECT®
Journal of Nuclear Materials 329–333 (2004) 1446–1450
journal of nuclear materials
www.elsevier.com/locate/jnucmat

Radiation-induced disordering in magnesium aluminate spinel subjected to ionizing radiation

M. Shimada [a,*], S. Matsumura [a], K. Yasuda [a], C. Kinoshita [a], Y. Chimi [b], N. Ishikawa [b], A. Iwase [b]

[a] *Department of Applied Quantum Physics and Nuclear Engineering, Kyushu University, Hakozaki 6-10-1, Fukuoka 812-8581, Japan*

[b] *Department of Materials Science, Japan Atomic Energy Research Institute (JAERI), Tokai, Ibaraki 319-1195, Japan*

Abstract

An analytical electron microscope study was carried out on single crystal specimens of magnesium aluminate spinel irradiated with 200 MeV Xe^{14+} ions up to 5.0×10^{15} and 2.0×10^{16} ions/m^2 at ambient temperature. Bright-field images showed structurally disordered columns of about 4–5 nm in diameter along ion tracks. Tiny pits were observed on the incident surface of the columns. Quantitative HARECXS analysis of atomic configurations revealed that disordering proceeds in more extended regions over 10 nm in diameter. The configurations of Al^{3+} ions are more disordered than that of Mg^{2+} ions. The disordered areas are appeared to overlap each other in the specimen irradiated with 2.0×10^{16} ions/m^2.

1. Introduction

Magnesium aluminate spinel ($MgO\cdot nAl_2O_3$) exhibits excellent irradiation resistance [1–3], especially to neutron irradiation. No significant swelling occurs in $MgO\cdot nAl_2O_3$ under neutron irradiation up to 2.5×10^{27} n/m^2 ($E>1$ MeV) at 658–1100 K [4]. In the spinel structure, O^{2-} ions form an fcc sublattice, and cations of Mg^{2+} and Al^{3+} occupy only 1/8 and 1/2 of the tetrahedral (IV) and the octahedral (VI) positions in the fcc sublattice. A considerable number of the remaining empty holes are believed to be attributable to the excellent resistance under radiation by accommodating displaced ions and suppressing aggregation of defects. The compounds are expected to be a candidate material for the inert matrix target material in nuclear transmutation of radioactive actinides [5,6]. In the applications, the materials will be subjected to a strong irradiation field yielding knock-on displacements as well as electronic excitation. The stability of the materials under such an irradiation field, should be understood in terms of the effects due to knock-on displacements and electronic excitation, respectively. Swift heavy ions considerably deposit their energy to ionization or electronic excitation than that to atomic collision. Especially in a thin foil specimen, the fraction of the latter events is very small. Therefore, the structural change in a thin film due to swift heavy ion irradiation is considered to result mostly from the electronic excitation processes.

For quantitative evaluations of local atomic configurations in irradiated materials, the present authors have developed high angular resolution electron channeling X-ray spectroscopy (HARECXS) in which characteristic X-ray emission is measured as a function of electron beam direction with high angular resolution. It has been demonstrated that the obtained profiles of X-ray intensity variations are very sensitive to crystallographic location of the elements [7,8].

The present paper reports quantitative TEM and HARECXS results on structural changes in

* Corresponding author. Tel.: +81-92 642 3773; fax: +81-92 642 3771.
E-mail address: shimaq@nucl.kyushu-u.ac.jp (M. Shimada).

0022-3115/$ - see front matter © 2004 Elsevier B.V. All rights reserved.
doi:10.1016/j.jnucmat.2004.04.161

$MgO \cdot nAl_2O_3$ ($n = 1.1$) induced by irradiation with 200 MeV Xe^{14+} ions, so as to clarify disordering behavior through high density electronic excitation.

2. Experimental

A single crystal of $MgO \cdot nAl_2O_3$ ($n = 1.1$) was cut into 3 mm diameter disks by an ultrasonic wave cutter, and the disks were mechanically polished to 120 μm thickness. The center part of the disks was dimpled and then subjected to 5 keV Ar^+ ion milling to achieve electron-transparent thin foils about 1 μm thick or thinner. The specimens were annealed at 1673 K for 2 h to remove radiation-induced defects introduced by ion milling. The annealed thin specimens were irradiated with 200 MeV Xe^{14+} ions to the fluence of 5.0×10^{15} or 2.0×10^{16} ions/m^2 at ambient temperature in a Tandem accelerator at Japan Atomic Energy Research Institute Tokai Laboratory. Fig. 1 shows SRIM [9] depth profiles of electronic stopping power S_e and displacement damage at a fluence of 2.0×10^{16} ions/m^2. Here displacement threshold energies were assumed to be 25, 20 and 60 eV for Mg, Al and O, respectively. In the TEM specimens as thin as 1 μm, Xe^{14+} ions deposit their energy mostly in the electronic system with a rate higher than 24 keV/nm. Knock-on displacements in the specimens are evaluated to be less than 10^{-4} dpa. The transmission electron microscope used in the experiments was an FEI TECNAI-20 equipped with an EDX system at the HVEM laboratory of Kyushu University. HARECXS experiments were carried out at 200 kV under excitation of systematic row of reflections $g = 400$. Characteristic X-ray signals of Mg–K, Al–K and O–K were measured as a function of incident beam direction between $-4g$ and $+4g$ Bragg positions. The illuminated areas in HARECXS experiments were about 1 μm in diameter.

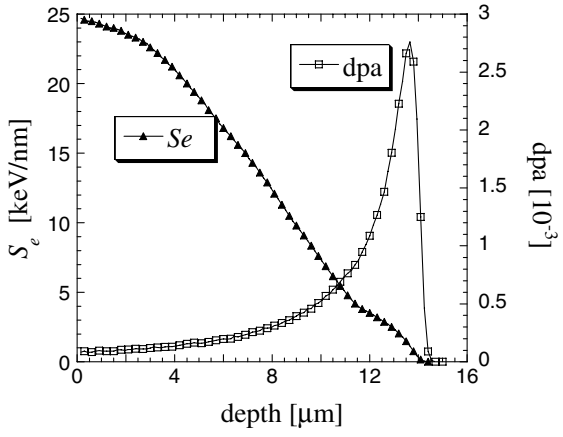

Fig. 1. Depth profiles of electronic stopping power (S_e) and dpa for 200 MeV Xe^{14+} ions calculated by SRIM code.

3. Results and discussion

3.1. Microstructure

Fig. 2 shows a plan-viewed bright-field image of a specimen, which was irradiated with 5.0×10^{15} ions/m^2. Dark dots about 3 nm in diameter appear over the whole area. The number density of dots is evaluated to be 3.5×10^{15} m^{-2}, which almost corresponds to the value of total dose of ions. Therefore, we consider that the contrast dot contrast arise from individual disordered columns formed along ion tracks. Fig. 3 gives bright-field images when the specimen was tilted by 20° from the direction of incident ions. The inclined view in the just focused condition in (b) exhibits columnar regions of dark contrast about 4–5 nm in width, which is somewhat broader than the dots observed in Fig. 2. If the image is defocused, distinct bright or dark dots appear at the entrance ends of ion tracks, as shown in Fig. 3(a) and (c). The contrast change suggests the presence of tiny pits, at the entrance of ion tracks. Such small pits have been often recognized on the surfaces subjected to swift heavy ion irradiation. AFM measurements revealed the geometry of pits formed at the surface of α-Al_2O_3 when irradiated with 269 MeV Bi [10]. Small hollows of 5 nm in diameter and 0.7 nm in depth are surrounded by hillocks of 1 nm in height. Similar holes are considered to be formed in the present case.

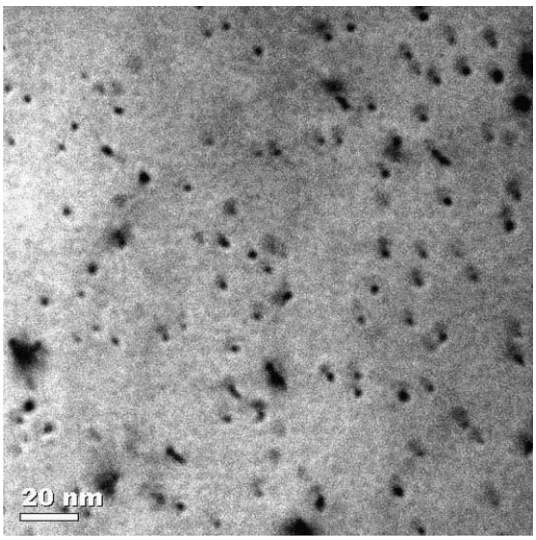

Fig. 2. Bright-field image of $MgO \cdot 1.1Al_2O_3$ irradiated with 200 MeV Xe^{14+} up to 5.0×10^{15} ions/m^2, which is a plan-view micrograph taken along the irradiation direction.

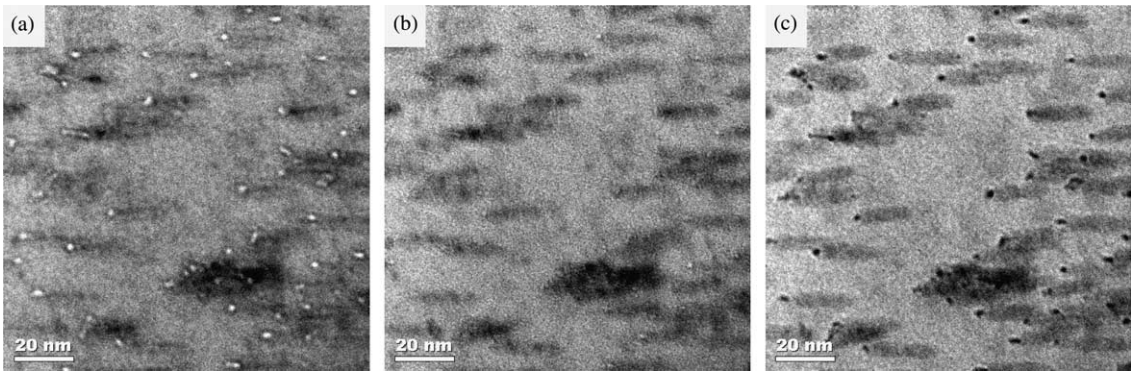

Fig. 3. Bright-field images ($0g/4g$, $g = 400$) of $MgO \cdot 1.1Al_2O_3$ irradiated with 200 MeV Xe^{14+} up to 5.0×10^{15} ions/m^2 in the conditions of (a) under-focus, (b) just-focus and (c) over-focus. The specimens were tilted by 20° from the incident direction of ions.

3.2. HARECXS analysis

X-ray emission of Mg–K, Al–K and O–K signals from an unirradiated specimen is given as a function of the incident electron beam direction in Fig. 4(a). Here, the intensities are normalized by the values under a kinematical diffraction condition. In this nomenclature, $k_x/g_{400} = 1$ corresponds to the exact Bragg condition with a 400 reflection. The intensities of Al–K and O–K are higher than that of Mg–K in the range $|k_x/g_{400}| < 1$, whereas Mg–K is enhanced in $1 < |k_x/g_{400}| < 2$. The spinel structure has alternative stacking of two types of 400 planes; one consists of only IV sites and the other does of VI and fcc sites. The HARECXS profiles in Fig. 4(a) clearly show that Mg^{2+} ions are preferentially located in the IV sites, and Al^{3+} and O^{2-} occupy the VI and fcc lattice sites. One can quantitatively determine atomic configurations in the crystal lattice by fitting simulated HARECXS profiles to the experimental ones, taking advantage of ICSC (Inelastic Cross Section

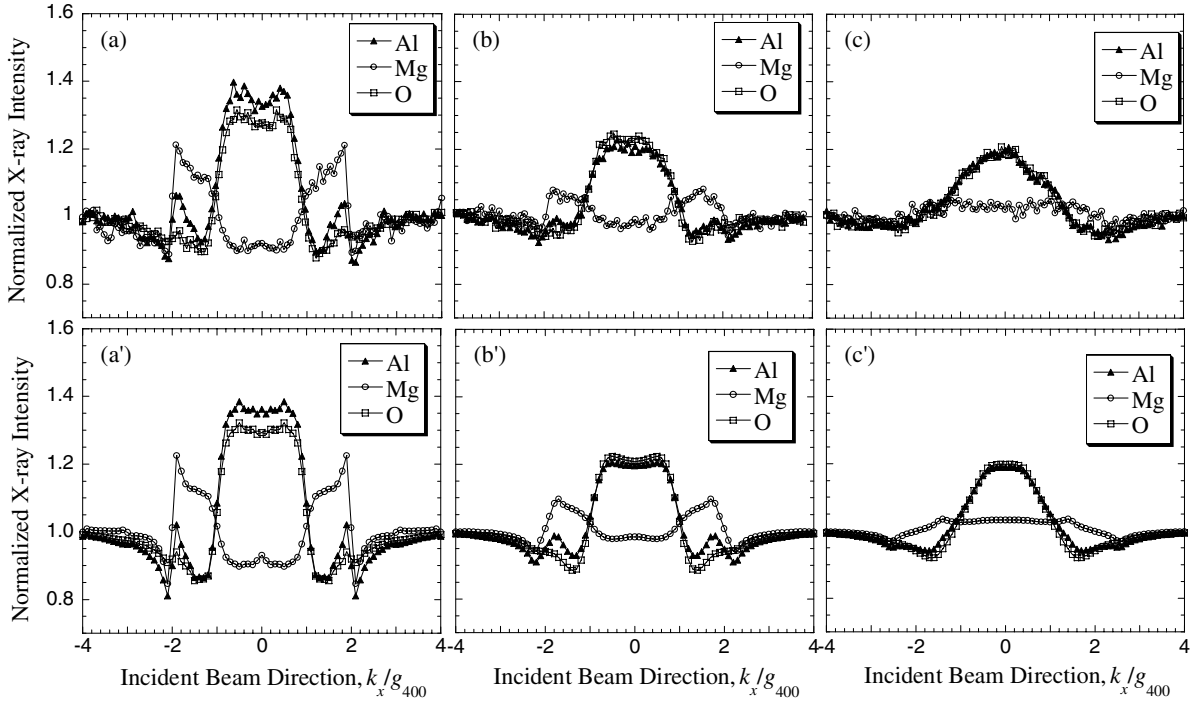

Fig. 4. Experimental HARECXS profiles of $MgO \cdot 1.1Al_2O_3$ (a) unirradiated, (b) irradiated with 200 MeV Xe^{14+} up to 5.0×10^{15} ions/m^2 and (c) 2.0×10^{16} ions/m^2. Simulated profiles of (a), (b) and (c) are shown in (a′), (b′) and (c′), respectively.

Table 1
Occupation probabilities of Mg^{2+}, Al^{3+} and O^{2-} on the IV sites, the VI sites and fcc sites in unirradiated $MgO \cdot 1.1Al_2O_3$ and irradiated with 200 MeV Xe^{14+} up to 5.0×10^{15} ions/m^2 and 2.0×10^{16} ions/m^2

	Mg^{2+}		Al^{3+}		O^{2-}	
	IV	VI/fcc	IV	VI/fcc	IV	VI/fcc
Unirradiated	0.72	0.28	0.15	0.85	0.00	1.00
5.0×10^{15} ions/m^2	0.62	0.38	0.26	0.74	0.02	0.98
2.0×10^{16} ions/m^2	0.52	0.48	0.26	0.74	0.04	0.96

Calculator) program [11] based on the dynamical diffraction theory [12,13]. The occupation probabilities for IV sites and VI/fcc sites thus obtained are listed in Table 1. It is indicated that the unirradiated $MgO \cdot nAl_2O_3$ ($n = 1.1$) has a partially disordered cation configuration, where about 28% of Mg^{2+} ions and 15% of Al^{3+} ions are located on their anti-sites.

The same analysis was applied to irradiated specimens. Fig. 4(b) and (c) shows the results after irradiation up to (b) 5.0×10^{15} and (c) 2.0×10^{16} ions/m^2. The X-ray intensity variations become less pronounced with increasing fluence, and there can be seen a different tendency for different elements. The Mg–K signal exhibits less dependence of k_x/g_{400}, whereas Al–K and O–K show still significant variations of intensity even after irradiation with 2.0×10^{16} ions/m^2. Good agreements between the experimental and the simulation profiles are obtained as shown in Fig. 4(b′) and (c′), with occupation probabilities of the three elements listed in Table 1. This indicates that Mg^{2+} ions are displaced from the IV sites to VI sites with increasing fluence. Almost the same amounts of Mg^{2+} ions are located at both sites after irradiation with 2.0×10^{16} ions/m^2. On the other hand, the Al^{3+} configuration changes significantly during irradiation up to 5.0×10^{15} ions/m^2, but not at higher fluence. Small amount of displacements of O^{2-} ions from the fcc lattice sites are also recognized, and the displacements increase with increasing fluence.

It should be noted that the occupation probabilities are averaged over an area of 1 μm diameter, where heavily disordered columns along with ion tracks and the less-affected matrix are consist. The total volume of ion track columns per unit volume (a) is given as

$$a = \pi r^2 A. \quad (1)$$

Here, r and A are the radius and the number density of ion tracks. If the disordering would occur only within the columns observed in Fig. 2, the volume fraction of disordered regions would attain only 7% at the fluence of 5.0×10^{15} ions/m^2. The fraction of disordered regions is too small to explain the significant change in atomic configurations as listed in Table 1. Hence, it should be considered that the disordering has taken place more extensively along the tracks. Here, we assume, as the first approximation, that there exist two regions with cation random arrangement in the unirradiated state, respectively. The expected profiles of HARECXS from the two phase state were calculated as a function of the volume fractions. Comparing the calculations to experimental profiles, the volume fractions of disordered regions of Mg^{2+} and Al^{3+} ions were evaluated about 30% and 60%, respectively, at a fluence of 5.0×10^{15} ions/m^2. It follows that Mg^{2+} and Al^{3+} ions take the disordered random arrangements over ranges 10.4 and 14.7 nm in diameter, respectively. The difference of the estimated disordering ranges suggests that Mg^{2+} and Al^{3+} ions would suffer the electronic excitation in different magnitudes, and the disordering of the two elements would proceed independently rather than cooperatively. The cation disordering can not be explained in the terms of a simple exchange with Mg^{2+} and Al^{3+}. The disordered regions are most likely to be overlapped at the fluence of 2.0×10^{16} ions/m^2. The degree of overlap should be different between the disordered zones of Mg^{2+} and Al^{3+}. This may explain why further disordering takes place with only Mg^{2+} but not with Al^{3+} ions during a prolonged irradiation from 5.0×10^{15} to 2.0×10^{16} ions/m^2.

4. Conclusions

In present study, conventional TEM observation and HARECXS analysis on ion configuration were employed to investigate structural changes in $MgO \cdot nAl_2O_3$ ($n = 1.1$) irradiated with 200 MeV Xe^{14+}. The main conclusions are drawn as follows:

(1) Irradiation with 200 MeV Xe^{14+} ions produces heavily disordered columns about 4–5 nm in diameter along the tracks with a high density electronic excitation of about 24 keV/nm. Tiny pits are formed at the entrance of ion tracks.
(2) Electronic excitation from one particle of 200 MeV Xe^{14+} causes significant disordering in region over 10 nm in diameter.
(3) The disordering of Al^{3+} ions takes place over a larger area than that of Mg^{2+} ions.
(4) The disordered zones overlap each other after irradiation up to 2.0×10^{16} ions/m^2.

Acknowledgements

The authors would like to express sincere thanks to Dr C.J. Rossouw (CSIRO) and Dr M.P. Oxley (University of Melbourne) for helpful discussion and comments on HARECXS analysis. This work was supported in part by Grant-In-Aid for Scientific Research (B) from the Japan Society for the Promotion of Science.

References

[1] C. Kinoshita, K. Fukumoto, K. Fukuda, F.A. Garner, G.W. Hollenberg, J. Nucl. Mater. 219 (1995) 143.
[2] F.W. Clinard Jr., G.F. Hurley, L.W. Hobbs, J. Nucl. Mater. 108&109 (1982) 655.
[3] S. Zinkle, C. Kinoshita, J. Nucl. Mater. 251 (1997) 200.
[4] C. Kinoshita, S. Matsumura, K. Yasuda, T. Soeda, M. Noujima, Mater. Res. Soc. Symp. Proc. 540 (1999) 287.
[5] Hj. Matzke, V.V. Rondinella, T. Wiss, J. Nucl. Mater. 274 (1999) 47.
[6] N. Chauvin, R.J.M. Konings, Hj. Matzke, J. Nucl. Mater. 274 (1999) 105.
[7] T. Soeda, S. Matsumura, C. Kinoshita, N.J. Zaluzec, J. Nucl. Mater. 283–287 (2000) 952.
[8] S. Matsumura, T. Soeda, N.J. Zaluzec, C. Kinoshita, Mater. Res. Soc. Symp. Proc. 589 (2001) 129.
[9] J.F. Ziegler, J.P. Biersak, U. Littmark, The Stopping and Range of Ions in Solids, Pergamon, New York, 1985.
[10] V.A. Skuratov, D.L. Zadorski, A.E. Efimov, V.A. Kuluev, Yu.P. Toporov, B.V. Mchedlishvili, Rad. Measur. 34 (2001) 571.
[11] M.P. Oxley, L.J. Allen, J. Appl. Crystallogr. 36 (2003) 940.
[12] L.J. Allen, T.M. Josefsson, C.J. Rossouw, Ultramicroscopy 55 (1994) 258.
[13] C.J. Rossouw, C.T. Forwood, M.A. Gibson, P.R. Miller, Micron 28 (1997) 125.